Study of the North West Cape electron belts observed by DEMETER satellite

Xinqiao Li, Yuqian Ma, Ping Wang, Huanyu Wang, Hong Lu, Xuemin Zhang, Jianping Huang, Feng Shi, Xiaoxia Yu, Yanbing Xu, et al.

▶ **To cite this version:**

Xinqiao Li, Yuqian Ma, Ping Wang, Huanyu Wang, Hong Lu, et al.. Study of the North West Cape electron belts observed by DEMETER satellite. Journal of Geophysical Research Space Physics, 2012, 117, A04201 (10 p.). 10.1029/2011JA017121 . insu-01179657

HAL Id: insu-01179657

https://hal-insu.archives-ouvertes.fr/insu-01179657

Submitted on 23 Jul 2015

HAL is a multi-disciplinary open access archive for the deposit and dissemination of scientific research documents, whether they are published or not. The documents may come from teaching and research institutions in France or abroad, or from public or private research centers.

L'archive ouverte pluridisciplinaire **HAL**, est destinée au dépôt et à la diffusion de documents scientifiques de niveau recherche, publiés ou non, émanant des établissements d'enseignement et de recherche français ou étrangers, des laboratoires publics ou privés.

Study of the North West Cape electron belts observed by DEMETER satellite

Xinqiao Li,[1] Yuqian Ma,[1] Ping Wang,[1] Huanyu Wang,[1] Hong Lu,[1] Xuemin Zhang,[2] Jianping Huang,[2] Feng Shi,[1] Xiaoxia Yu,[1] Yanbing Xu,[1] Xiangcheng Meng,[1] Hui Wang,[1] Xiaoyun Zhao,[1] and M. Parrot[3]

Received 1 September 2011; revised 23 January 2012; accepted 10 February 2012; published 3 April 2012.

[1] We analyzed observation data collected by the Instrument for the Detection of Particles (IDP) on board the DEMETER satellite during a period of 17 months in 2007 and 2008. In the meantime, the VLF transmitter located at North West Cape (NWC) ground station was shut down during 7 months and working for a total of 10 months. By an (on-off) method, our analysis for the first time revealed in detail the transient properties of the space electron precipitation belt which is induced by the man-made VLF wave emitted from NWC. We mapped the electron flux distribution and figured out the space regions that the NWC belt covered. The NWC electron spectrograms have been investigated in a wide range of the McIlwain parameter L (1.1–3.0). Furthermore, we obtained the averaged energy spectra of the NWC electrons within the drift loss cone and compared their characteristics during daytime and nighttime. Our results confirm the previous studies of the enhancement of NWC electrons, the wisp structure, and the day/night difference of the electron flux. In addition, more detailed information is provided. We provide not only evidence of a momentary flux enhancement up to 3 orders of magnitude but also a flux reduction at higher L shells with a maximum up to 60% of the original value. For the first time, the energy spectra of NWC electrons covering the entire IDP energy band are presented for both nighttime and daytime and are quantitatively compared. At the end, our results are discussed, and their agreement with the theory of wave-particle interactions is checked.

Citation: Li, X., et al. (2012), Study of the North West Cape electron belts observed by DEMETER satellite, *J. Geophys. Res.*, *117*, A04201, doi:10.1029/2011JA017121.

1. Introduction

[2] More than 30 years ago, it was shown that the VLF wave emitted by ground-based transmitters can cause precipitation of electrons from the radiation belt and that the process obeys the theory of wave-particle interactions. Subsequently, there have been numerous experimental observations and theoretical interpretations on this subject. *Bullough et al.* [1976] studied the ELF/VLF radiation at the altitude of the Ariel satellite and revealed the phenomenon of wave-particle interaction in the geomagnetic conjugate region in the opposite hemisphere ($2 < L < 3$). *Kimura et al.* [1983] found strong correlations between the 0.3–6.9 keV electron fluxes observed by the EXOS-B satellite and the 0.3–9 kHz VLF wave emitted by a ground transmitter at SIPLE.

[3] In the Stimulated-Emission-of-Energetic-Particles (SEEP) experiment conducted from May to September 1982 by turning the transmitter at the NAA ground station on and off at the timescale of seconds, *Imhof et al.* [1983] studied the instantaneous correlation between the VLF signal and the electron fluxes observed by a low-orbiting satellite. *Inan et al.* [1985] interpreted the observation of the SEEP experiment using the theory of wave-particle interaction. They proposed that the precipitation of particles was restricted by pitch angle distribution of those particles close to the loss cone.

[4] During the same period, *Poulsen et al.* [1993] studied the VLF wave propagation in the D layer of the ionosphere and proposed a multiple-mode three-dimensional model. *Abel and Thorne* [1998] claimed that in the inner radiation belt the electron flux reduction induced mainly by the VLF wave scattering causes the electron precipitation into the loss cone. Their theoretical calculations indicated that the energy of wave-particle resonance decreases with higher L values. Furthermore, *Horne et al.* [2005] studied the mechanism of electron acceleration in the outer radiation belt. Their studies indicate that these electrons could be accelerated to about MeV energy range by a VLF wave of several kHz and that

[1]Institute of High Energy Physics, Chinese Academy of Sciences, Beijing, China.
[2]Institute of Earthquake Science, China Earthquake Administration, Beijing, China.
[3]Laboratory of Physics and Chemistry of Environment and Space, CNRS, Orleans, France.

Copyright 2012 by the American Geophysical Union.
0148-0227/12/2011JA017121

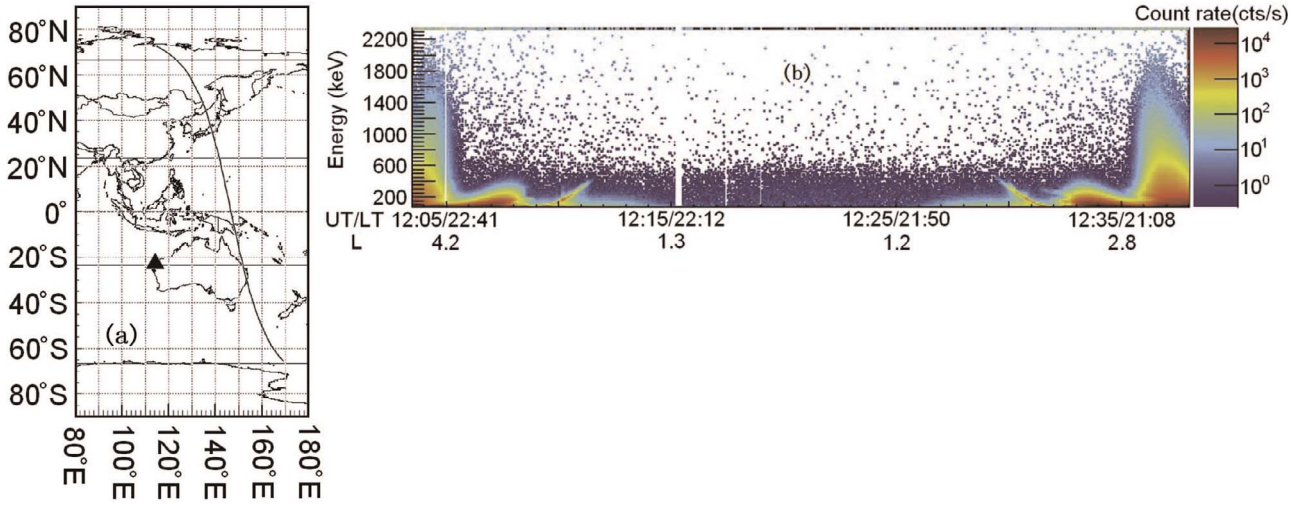

Figure 1. (a) Location of the NWC station (black triangle) and trajectory of the upward half orbit 20520. (b) Electron spectrogram versus UT/LT and *L* shell recorded along the orbit 20520.

the electron fluxes in the observed region could increase to 3 orders of magnitude within 1–2 days.

[5] The DEMETER satellite (Detection of Electro-Magnetic Emissions Transmitted from Earthquake Regions) launched in June 2004 is a low-altitude satellite with on board detectors to measure local electric and magnetic fields, energetic particle populations [*Sauvaud et al.*, 2006; *Berthelier et al.*, 2006; *Parrot et al.*, 2006], and additional quantities that are not utilized in the current study. These detectors provide us with the opportunity to further study the interaction between the man-made VLF waves and the particles in the radiation belt.

[6] By turning on and off the transmitter based at the NPM ground station, *Inan et al.* [2007] and *Graf et al.* [2009] studied the correlation between the ground VLF wave and the electron fluxes detected by the on board Instrument for Detecting Particles (IDP). The experiments were performed in 10 different timescales ranging from seconds to minutes, and they found correlations in 0.1 and 0.2 Hz on-off frequency [*Inan et al.*, 2007]. However, subsequent experiments using the 0.1 Hz frequency (i.e., on for 5 s and off for 5 s, alternately) indicated that the correlation rate is only 13.9% [*Graf et al.*, 2009]. Quite recently *Wang et al.* [2011] pointed out that this lower correlation rate may be due to the fact that IDP can only measure electrons with large pitch angles.

[7] Several authors studied the relation between the VLF emission from the North West Cape (NWC) transmitter and the electron flux observed by IDP, for the first time, in relatively larger space regions and longer time intervals. They show very strong ionosphere disturbance detected near the NWC ground station [*Parrot et al.*, 2007]. Moreover, due to the VLF wave emitted by the NWC transmitter, plenty of electrons, named "NWC electrons," are scattered into the drift loss cone, and they precipitate when they encounter the South Atlantic Anomaly (SAA). They covered a region with *L* values between 1.4 and 1.7 during the local night period. These studies also reported that the spectrum of NWC

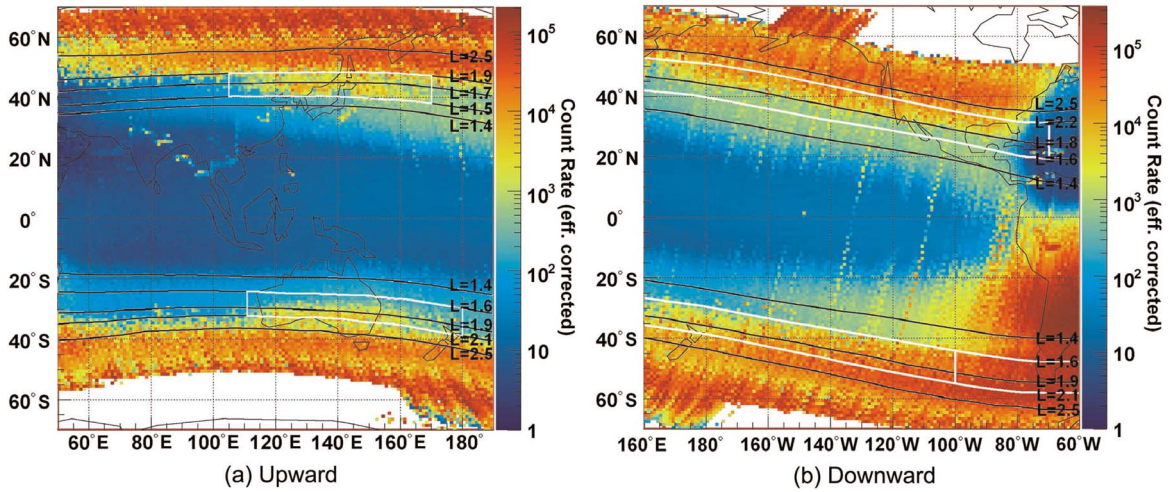

Figure 2. Electron flux distribution with the energy in the range of 108–411 keV during the whole year of 2008. Color scales indicate the average flux value within a pixel size of (1°, 1°). The simplified unit of counting rate (counts/s) is obtained by multiplying the factor of 1.16 (cm^2 sr) with the averaged flux value.

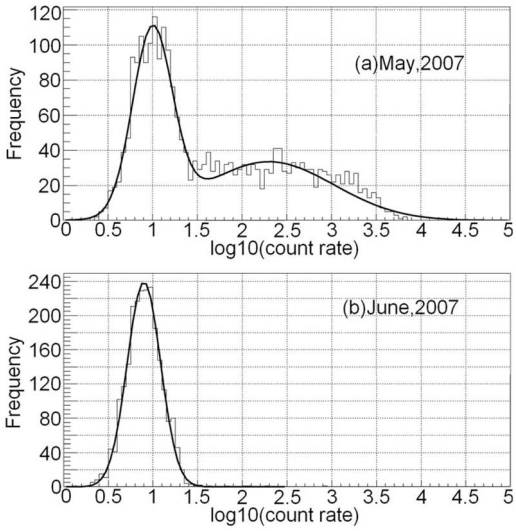

Figure 3. Statistical distribution of electron flux on logarithm scale, for local data (NL and SL) with an energy band of 206 ± 26.7 keV. The distribution in May has one more component with higher flux comparing with the one in June.

electrons has a wisp structure [*Sauvaud et al.*, 2008; *Gamble et al.*, 2008].

[8] There are also more relevant studies, for example, the numerical simulation for precipitation characteristics induced by five ground-based VLF transmitters [*Kulkarni et al.*, 2008], the restriction of VLF wave in (18–25 kHz) in driving electron precipitation from the inner radiation belt, as well as the effect of NAA station to electrons in the outer radiation belt [*Clilverd et al.*, 2008, 2010].

[9] Furthermore, recent studies have derived theoretical models of the NWC VLF wave transmission in the ionosphere [*Lehtinen and Inan*, 2009] and the different effect of ducted or nonducted VLF wave propagation [*Rodger et al.*, 2010]. A report revealed the increasing of the MF component at the height of the DEMETER orbit over the VLF transmitters [*Parrot et al.*, 2009]. This is a higher-frequency component of the whistlers produced by the global thunderstorm activity. Because the VLF transmitters induce ionospheric perturbations, the MF emissions can leak through the ionosphere with less attenuation at the VLF transmitter locations.

[10] We analyzed the IDP data which have been recorded during 2007 and 2008, when the NWC transmitter was turned off from June 2007 to February 2008 and turned on the rest of the time. The NWC transmitter has strong radiation power and very narrow bandwidth of the VLF emission. It provided us with the best opportunities for studying the mechanism of wave-particle interactions. In particular, because the NWC station was kept either on or off for a long period, we have enough data to make a comprehensive study about the effect of man-made electron precipitation with a high statistical significant level.

[11] In this work, an independent treatment has been made, for the first time, by using (on-off) method for the IDP in situ measurement data during 7 months of NWC off and 10 months of NWC on. The spatial distributions of NWC electrons have been figured out for different wisp regions. Energy spectra of NWC electrons in drift loss cone have been studied quantitatively. They have wisp structures and form "NWC electron belt," or "NWC belt" in brief. The NWC belt is a kind of instantaneous electron belt, which only appears during the NWC working period.

2. Statistical Analysis of the NWC Electron Flux

[12] The orbit of the DEMETER satellite is at the height of 670 km (after 2005). It is a quasi-Sun-synchronous orbit, and the orbital inclination is 98°. The satellite is three-axis stabilized. During local daytime the satellite flies downward (from north to south) and the descending node is 10:30 at noon; during local nighttime it flies upward (from south to north) and the ascending node is 22:15 at midnight. The orbital period is 102.86 min. The repeated period of an orbit location is around half of a month.

[13] The NWC ground station is located in the northwest corner of Australia at (21.82°S, 114.15°E). Its geomagnetic coordinate is (−31.96°, 186.4°). The NWC transmitter

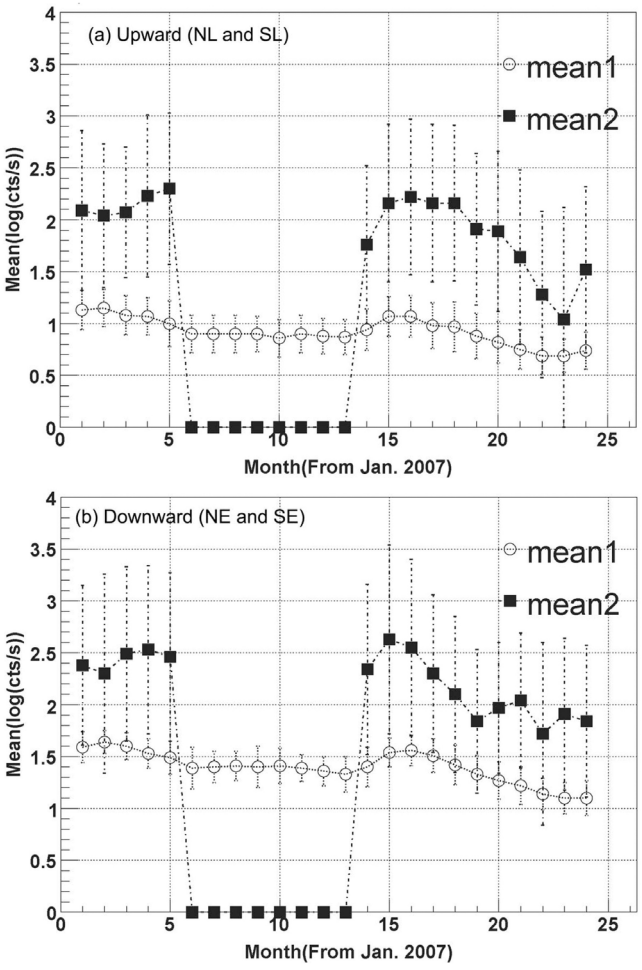

Figure 4. Fit result for monthly averaged electron fluxes. The mean and sigma of double/single Gaussian fit for each month of 2007 and 2008 are presented for (a) upward part and (b) downward part of the orbits. The circles represent the background component, and the black squares represent the signal component shown in Figure 3.

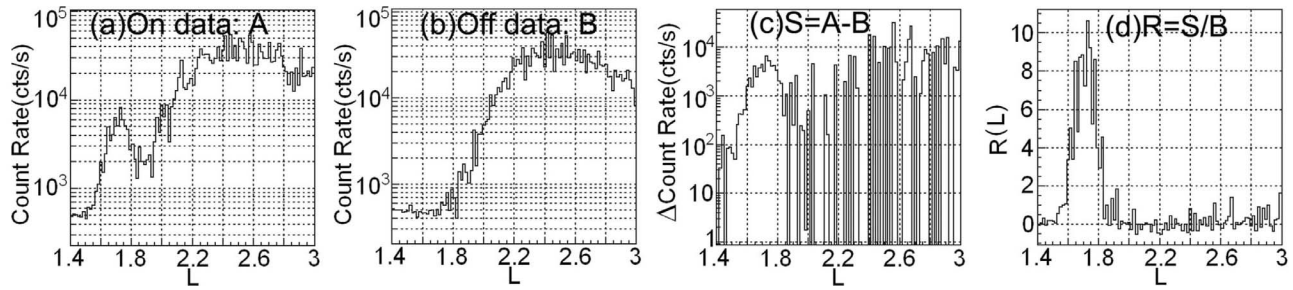

Figure 5. Averaged electron flux versus L in NL region, taking a longitude range of 105°–170° to get averaged flux. (a) Flux for NWC on, (b) flux for NWC off, (c), flux of signal with (on-off), and (d) ratio of signal to background.

works at 19.8 kHz with a very narrow bandwidth of 300 Hz and a large emission power of 1 MW.

[14] IDP was placed on the flank of the DEMETER satellite with a field of view (FOV) of 32°, which was pointing toward the west during the satellite upward flying at night and toward the east during the satellite downward flying at daytime. So most of the time, the electrons with big pitch angle close to 90° can be detected by IDP. Figure 1a shows the location of the NWC station and, as an example, the trajectory of a satellite orbit in east side. Figure 1b presents electron spectrogram detected by IDP all along this orbit. It should be noted that in Figure 1b there are two spectra with slanted wisp structure in the lower-energy bands around $L \sim 1.9$ in the south and $L \sim 1.6$ in the north, which correspond to the precipitated electron belt induced by the NWC VLF wave. These will be the focus of this study.

[15] We mapped the electron flux with the data covering the entire year of 2008. The electron flux in the energy band of 108–411 keV was averaged in each of the (1°, 1°) pixels along the geographic latitude and longitude. The result is shown in Figure 2. The white boxes delimit the main regions of the VLF man-made electron belts corresponding to the wisp structures shown in Figure 1b. The black lines mark the value of the McIlwain parameter L at the height of the DEMETER satellite. Figure 2a shows the range of the NWC electrons drift loss cone detected during the upward flying. Whereas during the downward flying, the NWC electrons were detected to move toward east, extending all the way to the South Atlantic Anomaly (SAA) region in the Southern Hemisphere, as shown in Figure 2b.

[16] The white boxed regions in Figure 2a which correspond to upward orbit data are named south local (SL) for the electron belt near NWC and north local (NL) for the conjugation position of NWC. Whereas the three white box regions in Figure 2b, which correspond to downward data, are named southeast (SE) region, northeast (NE) region and SE-SAA region which is the part of the SE region extending into the SAA region.

[17] Using upward orbit data, the same mapping has been made for each individual month in 2007 and 2008. We have found that the electron precipitation belts in NL and SL regions vanished from June 2007 to January 2008, so the statistical analysis has been made for each of 24 months and each of two data groups: local (NL + SL) and eastward (SE + NE), respectively.

[18] For the analysis we have selected a longitude range of λ in (110E°, 170E°) for local group, (170E°, 120W°) for eastward group, a same L value range of (1.6, 1.8), and an electron energy range of 206 ± 26.7 keV. The average counting rate are calculated in each of (ΔL, $\Delta\lambda$) with an unit size of (0.01, 1°) and accumulated to get the flux distributions within the selected regions.

[19] As an example, Figures 3a and 3b display the results with the data in May and June 2007 respectively, which can be fit by a double Gaussian distribution or a single Gaussian distribution in logarithm scale of averaged counting rate. Compared with the one in June, the distribution in May has one more component with a very wide range of higher counting rate with a maximum value $\sim 10^4$ counts/s, which can be more than 1000 times the average background value.

[20] Figure 4 shows the statistics result for each of the 24 months in the 2 years. We can find that it has two components: a background component (mean 1 ± sigma 1) with

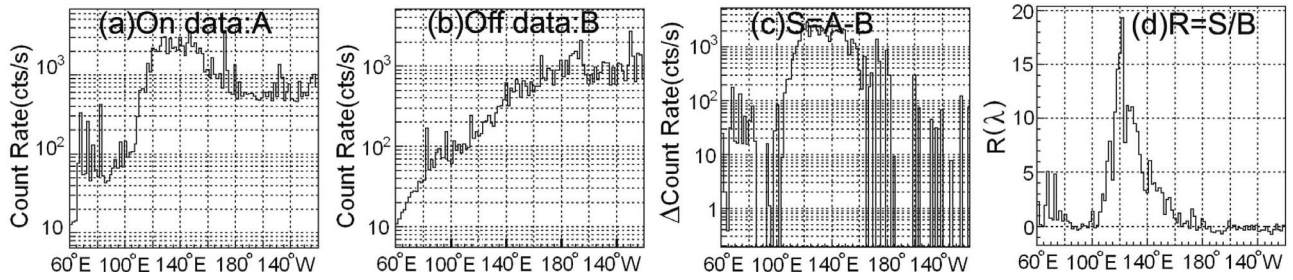

Figure 6. Averaged electron flux versus geolongitude in NL region, taking a L range of (1.5–1.9) to get averaged flux. (a) Flux for NWC on, (b) flux for NWC off, (c) flux of signal with (on-off), and (d) ratio of signal to background.

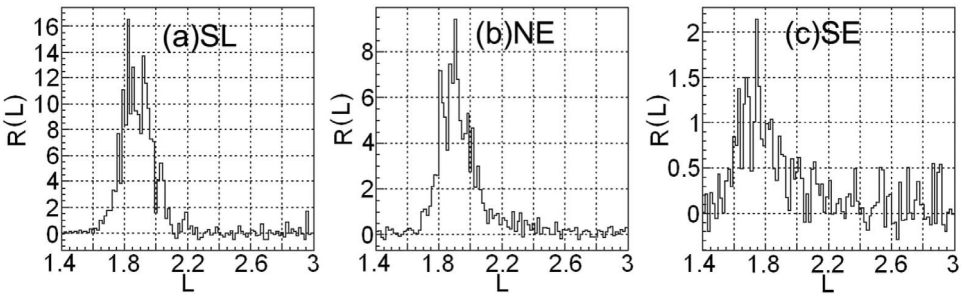

Figure 7. Ratio of signal to background $R(L)$ versus L value in the regions (a) SL, (b) NE, and (c) SE.

constant low counting rate and a high counting rate component (mean 2 ± sigma 2). This high counting rate component is distributed in a wide range and shows more variation. It vanished from June 2007 to January 2008 which is consistent with the NWC off time, i.e., the time when there was no signal from the NWC transmission as mentioned by *Zhang et al.* [2009]. So we can confirm that the component with high counting rate is contributed by the NWC transmission because its appearance and disappearance are clearly synchronized with the NWC on and off.

[21] The opposite pointing of IDP aperture during the upward and downward parts of the orbit may cause "east–west" effect during in situ measurement of electron fluxes. The difference is usually equal to around 16% in midlatitudes of Northern Hemisphere NL 0–28° [*Li et al.*, 2010]. The effect for NWC belts at higher latitudes can be estimated from Figures 4a and 4b. The differences of background fluxes between the two regions could be two times or more. A similar effect for the NWC electrons can also be seen in Figure 4.

[22] Based on the on and off status shown in Figure 4, we have selected "on data" and "off data," respectively. On data include the observations during 10 months from March to May 2007 and March to September 2008, while the off data include the observations during 7 months from July 2007 to January 2008. Since the solar activity was relatively quiet during 2007 and 2008, by subtracting the background "off data" from the "on data" (on-off), we can smooth out short-term random fluctuations. In addition, we can conduct detailed studies on the basic dynamic characteristics of the NWC electron belts using larger data sets to get better statistical significance. Since the electron flux varies every month and the NWC electrons are moving all the time, the results shown in sections 3 and 4 will reflect their average statistical properties.

3. Spatial Distribution of NWC Electrons

[23] We have selected the IDP data with electron energy in the 91–678 keV range, a L value between 1.4 and 3, and enough geolongitude range for the delimitation. The spatial distribution of NWC electrons have been quantitatively investigated with the (on-off) method. As an example, the results for the NL region are shown in Figures 5 and 6. The average counting rate of electrons were calculated for the whole given geolongitude range in each value of $L \sim L + \Delta L$. The results for on data (Figure 5a), off data (Figure 5b), signal (Figure 5a minus Figure 5b), and the ratio of signal to background R (L) were presented in Figure 5. Then the average counting rate of electrons were calculated for the whole 1.5–1.9 of L range in each of the geolongitude interval $\lambda \sim \lambda + \Delta\lambda$. The results for different conditions including the ratio of signal to background (S/B) of R (λ) are presented in Figure 6.

[24] Using the same treatment, the analysis for the other three regions (SL, NE, SE) were carried out. The results of R (L) and R (λ) for these regions are presented in Figures 7 and 8.

[25] It is clearly shown that the distributions of NWC electrons have very complicated profiles along the longitude and the magnetic shell. In the SE region, the effect of the NWC VLF wave expands up to ∼60°W of longitude, which is deeply into the SAA region due to the eastward drift of the NWC electrons. In the NE region the electrons drift stop at ∼80°W because they fall into SAA. With the high background electron flux in SAA, the NWC electrons still have a

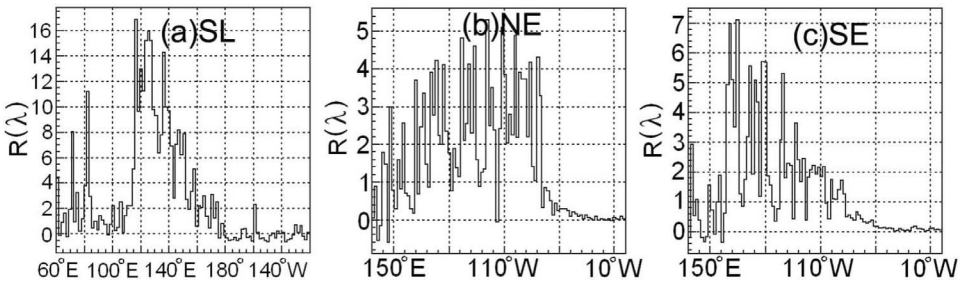

Figure 8. Ratio of signal to background $R(\lambda)$ versus geolongitude in the regions (a) SL, (b) NE, and (c) SE.

Table 1. The Main Area of the NWC Electron Belts (Wisp Range)

	NL	SL	NE	SE
L	1.5–1.9	1.6–2.1	1.6–2.2	1.6–2.1
$L@R(L)_{max}$	1.72	1.82	1.9	1.75
λ (deg)	105°E–170°E	110°E–180°E	155°E–80°W	150°E–60°W
$(\lambda)_{max}$ (deg)	120°E	115°E	125°E	170°E

S/B ratio of more than 1–2. In addition, the expansion effect of the radiation belt along magnetic shells up to $L \sim 3$ cannot be ignored. These sufficiently indicate that the VLF emission of the NWC transmitter powerfully influence the flux of the space electrons from the radiation belt.

[26] We define the ranges of the drift loss cone for NWC electrons belts according to R (L) and R (λ) distributions. Their characteristics are listed in Table 1.

[27] It is worth noting that the electron belts, related to NWC local region (SL and NL), correspond to the data measured during NWC local nighttime (on upward orbits). Oppositely, the belts, related to eastward region (SE and NE), correspond to the data measured during the local daytime (on downward orbits), which are only partially connected with the NWC nighttime. There is an overlapping longitude area in 150°E–180°E between the two regions. It may cause the different S/B ratio shown in Figures 8a and 8c because of the different data set and the different measurement period.

4. Energy Spectrum of NWC Electrons

[28] We have investigated the energy spectrum of the NWC electrons and its variation in various situations. The spectra were accumulated by on, off, and (on-off). The parameters taken for the investigation are basically selected according to Table 1.

4.1. Variation of Energy Spectrum Along With L Shell Value

[29] According to the results shown in section 3, we noted that at a certain altitude, the flux of NWC electrons varied with the L values of the satellite. The same effect exists for the energy spectrum. As an example, we present the result for NL region in Figure 9. The differential energy spectrum in three narrow ranges of L shell are presented for on, off, and (on-off) status, respectively. We first revealed that (1) within the NWC belt in the L range of 1.6–1.65, the flux of the NWC electrons has a peak centered at 220 keV with a S/B of 35; (2) for higher L region of 1.9–1.95, the electron enhancement is reduced and dominates in the range 300 keV to 1 MeV (it reaches a maximum value of S/B equal to ~1.3 near 600 keV); and (3) for region in inner radiation belt of the L range 2.05–2.1, a slot region is formed by the NWC electron flux reduction below 700 keV, with a S/B value reaching −60% near the peak of 300 keV. In all three cases, no NWC particle exists with energy above 1 MeV except the statistical fluctuation.

[30] In order to accurately investigate the evolvement of the NWC electron energy spectra along with L shell values, we have performed further study of spectrogram for the L shell with values from 1.3 to 3 in step size of 0.05 for the four NWC electron belts which have the longitude ranges shown in Table 1. The obtained results for both of enhanced and/or reduced electron fluxes from (on-off) value are displayed in Figure 10. Figure 10e concerns the "SE-SAA" region.

[31] From Figure 10, we can find the following characteristics of the NWC electron energy spectra:

[32] 1. In all five regions with electron precipitation, the spectra show obvious wisp structures in relative lower L shell range. The main part of the wisp structures correspond to NWC electron belts which have been defined in Table 1.

[33] 2. In local regions, there are obvious slot effects caused by electron loss in the energy range of 100–200 keV.

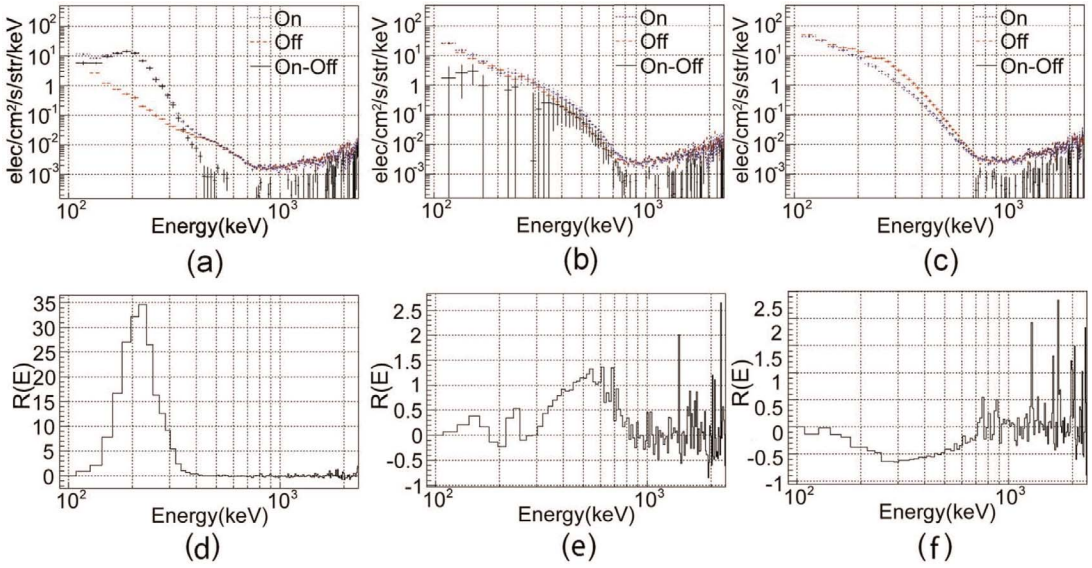

Figure 9. For NL region, energy spectra in the three cases of on, off, and on-off in the L ranges of (a) 1.6–1.65, (b) 1.9–1.95, and (c) 2.05–2.1. (d–f) The respective ratio of signal to background calculated by R = (on-off)/off in Figures 9a–9c.

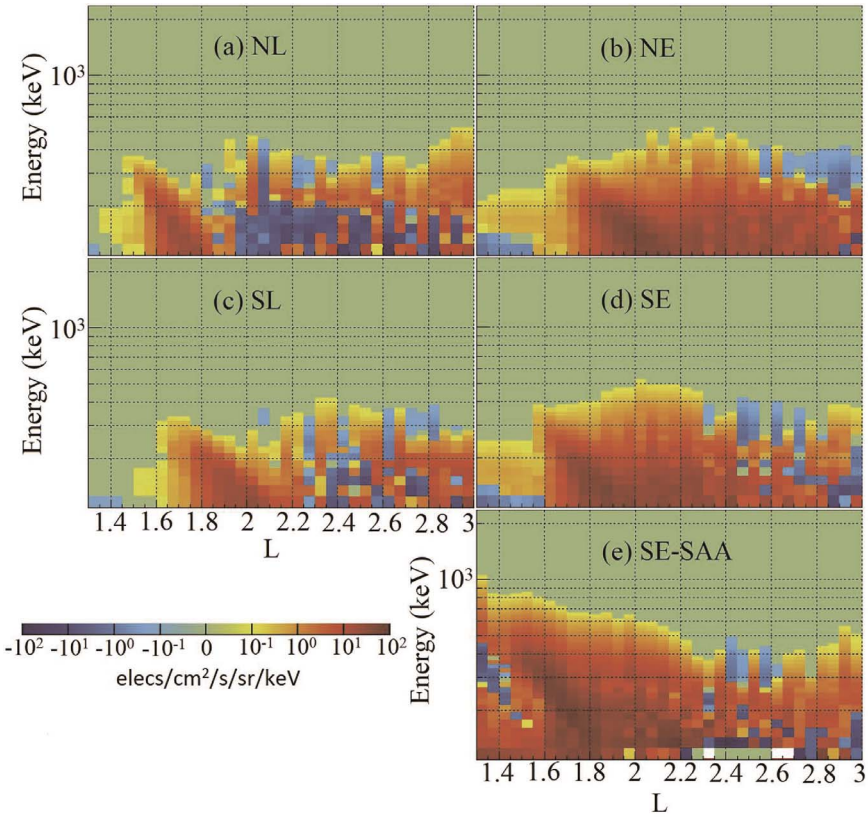

Figure 10. Spectrogram of the NWC electrons along with L values in five different regions. Figure 10e is for the SE-SAA region, which is an extension of the SE range with longitude of (100°W–60°W). Blue corresponds to a flux of (on-off) < 0. Here we set zero for $|flux| \leq 10^{-2}$ el cm^{-2} s^{-1} sr^{-1} keV^{-1}. Data with only statistical fluctuation have been ignored.

The electron loss is most obvious in the north region (NL) corresponding to L shell values equal to 1.95–2.5. The spectrum shows irregular structure in the south region (SL) with $L > \sim 2.2$.

[34] 3. In eastward regions, there is no obvious slot effect of NWC electrons. The enhancement in NE and SE regions with energy <300 keV extend to $L \sim 2.5$ and even to $L \sim 2.9$. The fluxes of lost electrons are rather lower; the distributions are mainly in the 300–400 keV range and slightly different for SE and NE.

[35] 4. SE-SAA is a special region which belongs to SAA and connects with SE at 100°W and collects a huge number of NWC electrons. It still keeps the wisp structure, but no belt feature is observed here due to the large background.

[36] Related to the physical mechanism, the common understanding is that the wisp structures should be most likely caused by local interactions between original 19.8 kHz of VLF wave and space electrons, which induce the electrons pitch angle scattering into the loss cone. The original VLF wave comes from the NWC transmitter by direct ducted propagation and causes wave-particle resonant interaction close to the geomagnetic equatorial plane. The fact that more electrons covered a wider L shell range in the eastward direction is due to the drift of precipitation electrons along with the longitude and the magnetic shell.

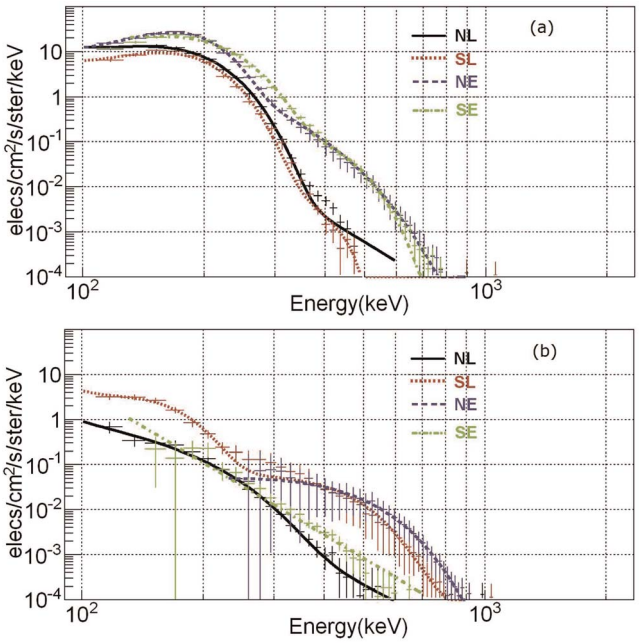

Figure 11. Differential energy spectra of the NWC electrons in the drift loss cone (a) for NWC nighttime and (b) for NWC daytime.

Table 2. Characteristics of Energy Spectrum of NWC Electron Belts During NWC Nighttime[a]

Area	Average Energy (keV)	Integrate Influence (10^{-4} erg cm^{-2} s^{-1} sr^{-1})	Integrated Flux (el cm^{-2} s^{-1} sr^{-1})
SL	169.8 (12.8)	2.68 (0.10)	986.8 (36.8)
NL	167.0 (11.1)	3.59 (0.12)	1344.1 (43.7)
SE	185.2 (8.5)	7.54 (0.17)	2543.5 (58.0)
NE	176.1 (7.4)	7.60 (0.16)	2696.2 (54.4)

[a]The values in parentheses are errors.

4.2. Differential Energy Spectrum of NWC Electrons and "Day-Night" Effect

[37] With the (on-off) method, we have obtained the total differential energy spectra of the NWC electrons, which are accumulated in each of the four regions defined in Table 1. Figure 11a presents the spectra related to NWC nighttime using upward data for SL and NL regions, and downward data for SE and NE regions. Figure 11b is the spectra related to NWC daytime using downward data for SL and NL regions, and upward data for SE and NE regions. For each spectrum, the average energy, the integrated energy density and the integrated flux density, as well as the differences of these physical parameters between NWC daytime and nighttime have been derived and listed in Tables 2 and 3, respectively.

[38] The following brief comments are about these results.

[39] 1. During NWC nighttime, spectrum features are different between local and eastward regions. The spectra in SL and NL regions have almost the same feature, with the same peak below ~200 keV and the same cutoff energy at ~500 keV. There is an enhancement of the electron flux in the eastward region and the cutoff energy increase to 800 keV. This phenomenon indicates the existence of a continuous process of the electron drift and a possible acceleration during this drift.

[40] 2. During NWC daytime, we still can see the NWC electrons, but the fluxes of electrons are rather weak, and the spectrum features are quite different with each other. The cutoff energies of the NL and SL regions increase to 600 and 700 keV, respectively. The flux in the SL region is strongest whereas it is weakest in the NE region. The spectra in the eastward region show more absorption of electrons during the drift, so that only electrons with E > 250 keV in the NE region can be observed. As we know that the average energy of resonant particles is ~180 keV within NE region during nighttime, so it at least implicates that the original VLF wave at 19.8 kHz almost cannot reach the NE region due to ionosphere daytime absorption.

5. Verification of Wave-Particle Theory From the Pitch Angle Distribution

[41] IDP has no ability to identify the pitch angle of incident particles. So, the direction between the axis of IDP aperture and the local magnetic field is taken as the pitch angle and recorded into the database. For each of the four NWC electron belts, we make the pitch angle distribution of incident electrons according to the data set, and as example, the histograms for NWC night in the NL and SL regions are presented in Figure 12. The actual distribution can be recovered by a fit of Gaussian function with a setting of 16° as 3σ of the FOV (see curves in Figure 12).

[42] The analysis shows that the distributions are quite different in different belt regions, as well as between NWC day and NWC night. But in all of the results, measurable electron pitch angles are distributed mostly within 60°–110°. At a latitude of 37°, it is mostly within 70°–90° which correspond to 23.5°–25° at the equator.

[43] The quasi-linear theory provides a quite complete description of fully ionized plasmas, and it offers a solid foundation for wave-particle interactions. This theory assumes that the wave amplitude is small enough so that the variation of particle distribution function with time is slow compared with the period of wave. Furthermore, if physical quantity (such as pitch angle) changes by only a small increment during each elemental interaction and wave phases have no correlation with each other, the behavior of particles can be treated as diffusion. After expanding a collisionless Vlasov equation for the particle distribution function to the second order in perturbation, the diffusion equation is obtained. In the inner radiation belt, for particles with velocities much larger than typical phase velocities of waves, the energy diffusion is negligible, and pitch angle diffusion plays a dominant role.

[44] In the inner radiation belt, based on resonant interaction after ignoring the energy diffusion, the quasi-linear diffusion equation (Fokker-Planck equation) can be written as [*Melrose*, 1980]

$$\frac{\partial f}{\partial t} = \frac{1}{\sin\alpha}\frac{\partial}{\partial \alpha}\left(D_{\alpha\alpha}\sin\alpha\frac{\partial f}{\partial \alpha}\right) \tag{1}$$

where f(α, E, L) is the density function in the phase space, which depends on the local pitch angle α, the kinetic energy E, and the McIlwain parameter L. $D_{\alpha\alpha}$ is the local pitch angle diffusion coefficient, which contains all information about wave-particle interactions. As for the NWC electrons with a given value of L shell and a kinetic energy E, the value of the local diffusion coefficient $D_{\alpha\alpha}$ relies on the pitch angle distribution.

[45] Local diffusion coefficient of resonant interaction between electrons and VLF waves can be written as [*Summers*, 2005]

$$D_{\alpha\alpha} = \frac{\pi}{2}\frac{\Omega_e}{\rho}\frac{1}{(E+1)^2}\sum_i \frac{\Delta b^2}{B^2}\frac{\left(1-\frac{x_i\cos\alpha}{y_i\beta}\right)^2\left|\frac{dx_i}{dy_i}\right|}{\delta x\left|\beta\cos\alpha-\frac{dx_i}{dy_i}\right|} \cdot \exp\left[-\left(\frac{x_i-x_m}{\delta_x}\right)^2\right] \tag{2}$$

Table 3. Characteristics of Energy Spectrum of NWC Electron Belts During NWC Daytime[a]

Area	Average Energy (keV)	Integrate Influence (10^{-4} erg cm^{-2} s^{-1} sr^{-1})	Integrated Flux (el cm^{-2} s^{-1} sr^{-1})	Flux Ratio (Night/Day)
SL	161.0 (31.7)	0.601 (0.065)	233.7 (20.8)	4.2
NL	157.7 (39.7)	0.096 (0.012)	38.0 (4.8)	35.4
SE	203.8 (109.5)	0.063 (0.016)	19.4 (5.4)	130.9
NE	378.6	0.071 (0.032)	11.7 (5.9)	231.1

[a]The values in parentheses are errors.

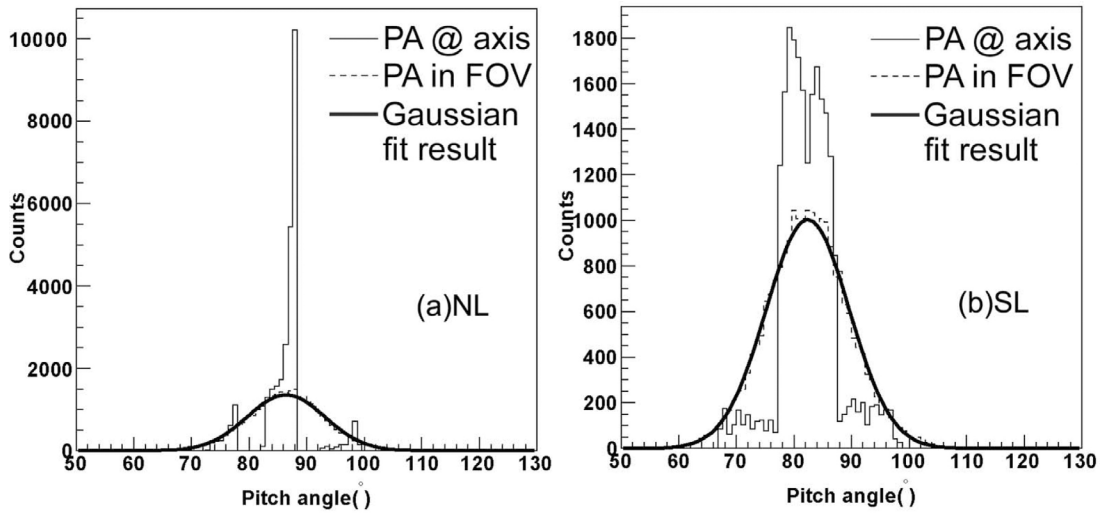

Figure 12. Pitch angle (PA) distributions of the NWC electrons in the (a) NL and (b) SL regions during NWC nighttime.

where $\beta = v/c$, B is the Earth's magnetic field and Ω_e is electron gyrofrequency; x_m and δx are reduced parameters defined as $x_m = \omega_m/\Omega_e$, $\delta_x = \delta\omega/\Omega_e$; x_i and y_i are reduced variables with $x_i = \omega_i/\Omega_e$, and $y_i = ck_i/\Omega_e$, respectively. Assuming that the wave-particle interaction mechanism occurs only within the equatorial plane and is valid for purely field-aligned wave propagation, we obtain the equatorial pitch angle diffusion coefficient.

[46] According to the DEMETER observations, to calculate equatorial pitch angle diffusion coefficient, parameters are chosen as follows: $\omega_m = 19.8$ kHz as the frequency of the maximum wave power, $\delta\omega = 150$ Hz and the wave amplitude $\Delta b = 10$ pT. The equatorial magnetic field is given by a dipole model $B = 3.11 \times 10^5/L^3$ T and the equatorial plasma density N_0 is equal to $880 \times (2/L)^4$ cm^{-3} according to *Angerami and Thomas* [1964] and *Inan et al.* [1984].

[47] From Figure 13, we see that electron pitch angles are just within or nearby the FOV range of IDP. As a result, the electrons which participate to the interaction with the VLF wave transmitted by NWC are observed by DEMETER during this process. Thus, the observed "NWC man-made radiation belt" can be explained by pitch angle diffusion based on a resonant interaction.

6. Summary and Discussion

[48] Based on DEMETER IDP observations at the altitude of 670 km, the characteristics of the electron precipitation, induced by VLF wave emission from the NWC station, have been quantitatively studied in detail. With the long-term observation data related to NWC on and off, the background can be eliminated by an (on-off) method with high reliable statistics. For the first time, the space distributions, the spectrogram via L shells, and the differential energy spectra of the NWC electrons have been obtained.

[49] The results based on NWC night data indicate that at 670 km height, the NWC VLF wave induced significant enhancement of electrons flux within drift loss cone. It forms two temporary electron belts: one in the south starts from the west of NWC station (110°E) and extends to the SAA (60°W); the other is in the north at its conjugate position, starts from ~105°E and ends at ~80°W. Each belt is related to two sets of in situ measurement data, which present two kinds of properties. So, in total four belt regions, SL and NL for local region and SE and NE for eastward region, have been separately studied.

[50] The SL and NL belts are mainly associated with a direct interaction between the electrons and the VLF wave emitted by the NWC transmitter. They are only formed during the NWC nighttime. Two belts covered a longitude range of 60°–70°, which have a dimension similar to the region where the ducted NWC VLF wave is observed. The spectrum and the distribution along with L shell are similar to each other. The eastward SE and NE belts are mainly formed by drift electrons, which covered a wide longitude range with about 135° for NE, and 150° for SE, and can be

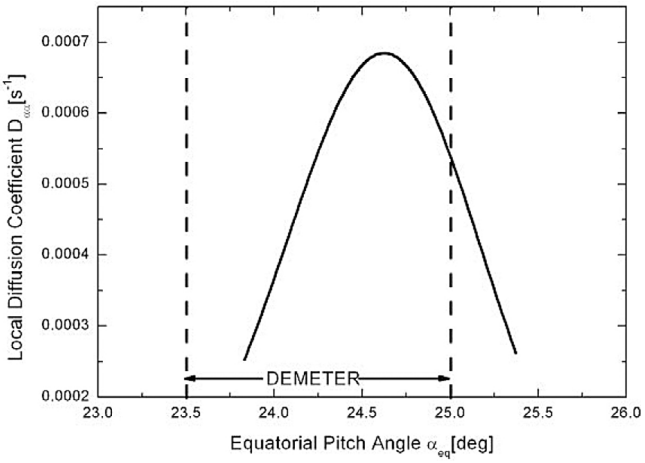

Figure 13. Local pitch angle diffusion coefficient as a function of the equatorial pitch angle for given L and E values. The area between the two vertical lines corresponds to electrons with pitch angle ranging from 23.5° to 25° at the equator which is 70°–90° at $L = 1.8$ observed by DEMETER. The electron's kinetic energy is $E = 220$ keV.

observed only by the set of downward data. The spectra show increases both in electron energy and flux along with *L* shell.

[51] Similar spectrum analyses have also been made for NWC daytime by using the other half orbit of data. Although the electrons flux is rather weak and the belt structure in drift loss cone vanished due to the ionosphere variation, but one still can see the spectrum, and compare the daytime-nighttime effects quantitatively.

[52] The electron precipitation, where flux enhancement arising within loss cone, can be explained by pitch angle scattering of the electrons, which is caused by wave-particle resonance interactions. This phenomenon is a kind of dynamic balanced process of the electron flux variations. It depends on which process is dominant for the electron flux either being enhanced locally from pitch angle diffusion or precipitation into the atmosphere.

[53] It is worth paying attention to the fact that at the altitude of DEMETER satellite, the man-made VLF wave can produce plenty of electron flux enhancement and that enhancement dominates compared with the precipitation, i.e., the electron loss.

[54] **Acknowledgments.** This work is based on observations with the electric field experiment ICE and the energetic particle experiment IDP embarked on DEMETER, which is operated by the Centre National d'Etudes Spatiales (CNES). The authors thank J. J. Berthelier, the PI of ICE, and J.A. Sauvaud, the PI of IDP for the use of the data. We are grateful to Shaoxie Xu, Jiadong Qian, Xuhui Shen and Zhenxia Zhang for useful discussions. This work was also supported by National High-tech R&D Program of China (863 Program) (2007AA12Z133).

[55] Robert Lysak thanks Roberto Battiston and another reviewer for their assistance in evaluating this paper.

References

Abel, B., and R. M. Thorne (1998), Electron scattering loss in Earth's inner magnetosphere: 1. Dominant physical processes, *J. Geophys. Res.*, *103*, 2385–2396.

Angerami, J. J., and J. O. Thomas (1964), Studies of planetary atmospheres: 1. The distribution of electrons and ions in the Earth's exosphere, *J. Geophys. Res.*, *69*, 4537–4560, doi:10.1029/JZ069i021p04537.

Berthelier, J. J., et al. (2006), ICE, the electric field experiment on DEMETER, *Planet. Space Sci.*, *54*, 456–471.

Bullough, K., A. R. L. Tatnall, and M. Denby (1976), Man-made e.l.f./v.l.f. emissions and the radiation belts, *Nature*, *260*, 401–403, doi:10.1038/260401a0.

Clilverd, M. A., C. J. Rodger, R. Gamble, N. P. Meredith, M. Parrot, J.-J. Berthelier, and N. R. Thomson (2008), Ground-based transmitter signals observed from space: Ducted or nonducted?, *J. Geophys. Res.*, *113*, A04211, doi:10.1029/2007JA012602.

Clilverd, M. A., C. J. Rodger, R. J. Gamble, T. Ulich, T. Raita, A. Seppälä, J. C. Green, N. R. Thomson, J. Sauvaud, and M. Parrot (2010), Ground-based estimates of outer radiation belt energetic electron precipitation fluxes into the atmosphere, *J. Geophys. Res.*, *115*, A12304, doi:10.1029/2010JA015638.

Gamble, R. J., C. J. Rodger, M. A. Clilverd, J.-A. Sauvaud, N. R. Thomson, S. L. Stewart, R. J. McCormick, M. Parrot, and J.-J. Berthelier (2008), Radiation belt electron precipitation by man-made VLF transmissions, *J. Geophys. Res.*, *113*, A10211, doi:10.1029/2008JA013369.

Graf, K. L., U. S. Inan, D. Piddyachiy, P. Kulkarni, M. Parrot, and J. A. Sauvaud (2009), DEMETER observations of transmitter-induced precipitation of inner radiation belt electrons, *J. Geophys. Res.*, *114*, A07205, doi:10.1029/2008JA013949.

Horne, R. B., et al. (2005), Wave acceleration of electrons in the Van Allen radiation belts, *Nature*, *437*, 227–230, doi:10.1038/nature03939.

Imhof, W. L., J. B. Reagan, H. D. Voss, E. E. Gaines, D. W. Datlowe, J. Mobilia, R. A. Helliwell, U. S. Inan, J. Katsufrakis, and R. G. Joiner (1983), Direct observation of radiation belt electrons precipitated by the controlled injection of VLF signals from a ground-based transmitter, *Geophys. Res. Lett.*, *10*, 361–364, doi:10.1029/GL010i004p00361.

Inan, U. S., H. C. Chang, and R. A. Helliwell (1984), Electron precipitation zones around major ground-based VLF signal sources, *J. Geophys. Res.*, *89*, 2891–2906, doi:10.1029/JA089iA05p02891.

Inan, U. S., H. C. Chang, R. A. Helliwell, W. L. Imhof, J. B. Reagan, and M. Walt (1985), Precipitation of radiation belt electrons by man-made waves: A comparison between theory and measurement, *J. Geophys. Res.*, *90*, 359–369, doi:10.1029/JA090iA01p00359.

Inan, U. S., M. Golkowski, M. K. Casey, R. C. Moore, W. Peter, P. Kulkarni, P. Kossey, E. Kennedy, S. Meth, and P. Smit (2007), Subionospheric VLF observations of transmitter-induced precipitation of inner radiation belt electrons, *Geophys. Res. Lett.*, *34*, L02106, doi:10.1029/2006GL028494.

Kimura, I., H. Matsumoto, T. Mukai, K. Hashimoto, T. F. Bell, U. S. Inan, R. A. Helliwell, and J. P. Katsufrakis (1983), EXOS-B/Siple Station VLF wave-particle interaction experiments: 1. General description and wave-particle correlations, *J. Geophys. Res.*, *88*, 282–294, doi:10.1029/JA088iA01p00282.

Kulkarni, P., U. S. Inan, T. F. Bell, and J. Bortnik (2008), Precipitation signatures of ground-based VLF transmitters, *J. Geophys. Res.*, *113*, A07214, doi:10.1029/2007JA012569.

Lehtinen, N. G., and U. S. Inan (2009), Full-wave modeling of transionospheric propagation of VLF waves, *Geophys. Res. Lett.*, *36*, L03104, doi:10.1029/2008GL036535.

Li, X. Q., et al. (2010), Observation of particle on space electro-magnetic satellite during Wenchuan earthquake (in Chinese), *Chin. J. Geophys.*, *53*(10), 2337–2344, doi:10.3969/j.issn.0001-5733.

Melrose, D. B. (1980), *Plasma Astrophysics*, Gordon and Breach, New York.

Parrot, M., et al. (2006), The magnetic field experiment IMSC and its data processing onboard DEMETER: Scientific objectives, description and first results, *Planet. Space Sci.*, *54*, 441–455.

Parrot, M., J. A. Sauvaud, J. J. Berthelier, and J. P. Lebreton (2007), First in-situ observations of strong ionospheric perturbations generated by a powerful VLF ground-based transmitter, *Geophys. Res. Lett.*, *34*, L11111, doi:10.1029/2007GL029368.

Parrot, M., U. S. Inan, N. G. Lehtinen, and J. L. Pinçon (2009), Penetration of lightning MF signals to the upper ionosphere over VLF ground-based transmitters, *J. Geophys. Res.*, *114*, A12318, doi:10.1029/2009JA014598.

Poulsen, W. L., U. S. Inan, and T. F. Bell (1993), A multiple-mode three-dimensional model of VLF propagation in the Earth-ionosphere waveguide in the presence of localized D region disturbances, *J. Geophys. Res.*, *98*, 1705–1717, doi:10.1029/92JA01529.

Rodger, C. J., B. R. Carson, S. A. Cummer, R. J. Gamble, M. A. Clilverd, J. C. Green, J.-A. Sauvaud, M. Parrot, and J.-J. Berthelier (2010), Contrasting the efficiency of radiation belt losses caused by ducted and nonducted whistler-mode waves from ground-based transmitters, *J. Geophys. Res.*, *115*, A12208, doi:10.1029/2010JA015880.

Sauvaud, J. A., T. Moreau, R. Maggiolo, J.-P. Treilhou, C. Jacquey, A. Cros, J. Coutelier, J. Rouzaud, E. Penou, and M. Gangloff (2006), High-energy electron detection onboard DEMETER: The IDP spectrometer, descripsion and first results on the inner belt, *Planet. Space Sci.*, *54*, 502–511, doi:10.1016/j.pss.2005.10.019.

Sauvaud, J.-A., R. Maggiolo, C. Jacquey, M. Parrot, J.-J. Berthelier, R. J. Gamble, and C. J. Rodger (2008), Radiation belt electron precipitation due to VLF transmitters: Satellite observations, *Geophys. Res. Lett.*, *35*, L09101, doi:10.1029/2008GL033194.

Summers, D. (2005), Quasi-linear diffusion coefficients for field-aligned electromagnetic waves with applications to the magnetosphere, *J. Geophys. Res.*, *110*, A08213, doi:10.1029/2005JA011159.

Wang, P., et al. (2011), The remendiation of radiation belt electrons caused by ground base man-made VLF wave, *Acta Phys. Sin.*, *60*, 23–28.

Zhang, X. M., et al. (2009), Ionosphere VLF electric field anomalies before Wenchuan M 8 earthquake (in Chinese), *Chin. J. Radio Sci.*, *24*(6), 1024–1032.

J. Huang and X. Zhang, Institute of Earthquake Science, China Earthquake Administration, Beijing 100036, China.

X. Li, H. Lu, Y. Ma, X. Meng, F. Shi, H. Wang, H. Wang, P. Wang, Y. Xu, X. Yu, and X. Zhao, Institute of High Energy Physics, Chinese Academy of Sciences, 19B, Yuquan Rd., Beijing 100049, China. (lixq@ihep.ac.cn; mayq@ihep.ac.cn; pwang@ihep.ac.cn)

M. Parrot, Laboratory of Physics and Chemistry of Environment and Space, CNRS, 3A Av. de la Recherche Scientifique, F-45071 Orléans CEDEX 2, France.